

Straight to the Source: Detecting Aggregate Objects in Astronomical Images with Proper Error Control

David A. Friedenber^g and Christopher R. Genovese

Abstract

The next generation of telescopes will acquire terabytes of image data on a nightly basis. Collectively, these large images will contain billions of interesting objects, which astronomers call *sources*. The astronomers' task is to construct a catalog detailing the coordinates and other properties of the sources. The source catalog is the primary data product for most telescopes and is an important input for testing new astrophysical theories, but to construct the catalog one must first detect the sources. Existing algorithms for catalog creation are effective at detecting sources, but do not have rigorous statistical error control. At the same time, there are several multiple testing procedures that provide rigorous error control, but they are not designed to detect sources that are aggregated over several pixels. In this paper, we propose a technique that does both, by providing rigorous statistical error control on the aggregate objects themselves rather than the pixels. We demonstrate the effectiveness of this approach on data from the Chandra X-ray Observatory Satellite. Our technique effectively controls the rate of false sources, yet still detects almost all of the sources detected by procedures that do not have such rigorous error control and have the advantage of additional data in the form of follow up observations, which will not be available for upcoming large telescopes. In fact, we even detect a new source that was missed by previous studies. The statistical methods developed in this paper can be extended to problems beyond Astronomy, as we will illustrate with an example from Neuroimaging.

Keywords: Blind Source Detection, Multiple Testing, Astrostatistics

David Friedenber^g is Doctoral Student, Department of Statistics, Carnegie Mellon University, Pittsburgh PA 15213 (E-mail:dfrieden@stat.cmu.edu). Christopher Genovese is Professor, Department of Statistics, Carnegie Mellon University, Pittsburgh PA 15213 (E-mail:genovese@stat.cmu.edu). This work is supported by National Science Foundation (NSF) grants 486560 and DMS0806009, National Institute of Health (NIH) grant 1R01NS047493, National Aeronautics and Space Administration (NASA) grant NNX07AH61G and the Bruce and Astrid McWilliams Center for Cosmology. The authors would like to thank Arthur Kosowsky and Neelima Seghal for the Atacama Cosmology Telescope data, Peter Freeman for his help with the Chandra X-ray telescope data, David Heeger and Eli Merriam for the fMRI data, and Rebecca Nugent, Chad Schafer, and Larry Wasserman for their helpful discussions.

1 Introduction

The typical astronomical image records the intensity of light, over some range of frequencies, across a section of sky that contains many celestial objects of various size, shape, and luminosity. The image's pixels correspond to an array of light-sensitive detectors in the telescope, and each pixel essentially counts how many photons have struck the corresponding detector during the exposure. But the photons recorded in the image do not come solely from the objects of interest, or *sources*; thermal noise and background emissions (collectively called *background*) corrupt the data and obscure the signature of the objects. Moreover, diffraction and atmospheric effects blur the image, reducing resolution and washing out the fainter signals. In the (astronomical) source detection problem, one is given such an image and seeks to construct a *catalog* that gives the coordinates (and often other properties) of sources in the image.

A source catalog is the basic data product of most astronomical surveys and the basic input to the scientific process. This has been true for some time. Early catalogs – from the data of ancient astronomers Shi Shen and Hipparchus, each cataloging about 1000 stars, to the compendium of deep-sky objects produced by William and Caroline Herschel in the 1700s (Herschel, 1786) – were based on direct visual observations. Later work, especially in the 20th century, used photographic plates, both improving resolution and allowing the detection of much fainter objects. But either way, compiling a source catalog would be a slow and painstaking affair, often requiring years to collect data on only a handful of objects. Until recently, catalogs comprising a few hundred objects were large, a few thousand were epic.

All this changed with the advent of new technologies – digital imaging, advanced designs for telescope mirrors, and computer automation – and with increases in available computing power and storage. With relative suddenness, astronomers found that they could observe wider, deeper, and faster than ever before. They could sweep the sky searching automatically for objects of a certain type, they could collect data on many objects in parallel, and they could observe a multitude of faint objects that would previously have gone undetected. The Sloan Digital Sky Survey (York et al., 2000) has measured hundreds of millions of objects. The upcoming Large Synoptic Survey Telescope (LSST, (Tyson and the LSST Collaboration, 2002)) will scan the entire sky every few days, collecting several terabytes of data per night into a catalog comprising *billions* of objects. Over the past two decades, astronomy has gone from data poor to data rich.

And therein lies both opportunity and challenge. The opportunity lies in the richness and importance of the scientific questions that these massive data sets can answer. The challenge lies in the sheer scale of the data analysis. While as a general rule in science, more data is better, there is a reason that astronomers often describe the coming bounty of data in quasi-biblical terms – a flood, a tsunami, an onslaught. The next generation of astronomical catalogs, including the LSST, will be so large that even simple operations – such as a basic query of the entire catalog – will be computationally prohibitive, and yes that does account for Moore's law.

This influx of data has motivated several statistical innovations in the field of Astronomy leading to the emergence of the sub-field, astrostatistics. New statistical innovations have had a significant impact on several important and cutting edge Astronomy problems, for a small sampling see van Dyk et al. (2009), Loredo (2007), Meinshausen and Rice (2006),

Genovese et al. (2004), and Richards et al. (2009).

Besides the massive size of the data, another issue is controlling the rate of errors in the catalog. In the past, where every object in the catalog was observed manually, sources were often missed, located incorrectly, or created spuriously. Follow-up observations can often be made for all or most of the sources, reducing false positive and false negative identifications to a manageable level. But in the near future, the sheer number of objects in the catalog will preclude comprehensive follow-up observations by human beings. Scientific studies of the catalog will likely need to be based on samples or selections made by automatic, statistical criteria. But no matter how carefully these criteria are constructed, there will be objects that are misclassified. To use the resulting samples effectively for scientific inference, it will be necessary for the method to provide tunable control of error rates. Thus, new statistical and computational methods will be needed to construct and analyze the next generation of astronomical source catalogs.

In this paper, we develop a multiple-testing-based method for the source detection problem that has several advantages over existing techniques, especially for the analysis of large-scale surveys like the LSST. Although we discuss our method in the context of astronomical source detection, the method applies to a wide range of similar problems such as neuroimaging (e.g. Buckner, 1998) and remote sensing (e.g. Richards and Jia, 1999), and we give such an example in a later section.

We assume that the input image is an $n \times m$ array of pixels, with the value recorded at pixel (i, j) denoted by Y_{ij} . The photons that contribute to Y_{ij} arise from two components: *sources*, the emissions produced by the celestial objects of interest, and *background*, which includes thermal noise, the emissions of unresolved objects, interfering radiation sources, atmospheric emissions, and all other anomalies or artifacts. astronomical images essentially measure photon counts for which a Poisson model is appropriate (Cash, 1979). So for our base model, we assume that the Y_{ij} 's are independent with

$$Y_{ij} \text{ distributed as } \text{Poisson}\langle \lambda_{1,ij} + \lambda_{0,ij} \rangle, \quad (1)$$

where $\lambda_{1,ij} \geq 0$, $\lambda_{0,ij} \geq 0$ denote the mean intensity of sources and background, respectively and $\lambda_{1,ij} + \lambda_{0,ij} > 0$. The idea here is that the pixels are measuring the counts in disjoint cells of a Poisson random field across the sky. This applies to good approximation for space-based observations like those reported in Section 2. For ground-based observation, the image is in addition blurred by atmospheric turbulence, so the Y_{ij} 's are no longer strictly independent. However, the Poisson model in Equation 1 still holds to reasonable approximation. In data sets where the counts are high, the Poisson random field can be further approximated by a Gaussian random field. In this paper, we utilize a technique originally developed for the Gaussian model and generalize it so that we can accommodate a wide variety of models.

The source detection problem is to identify which pixels contains sources and thus to separate the sources from the background. If $\lambda_{1,ij} > 0$, then we take pixel (i, j) to be a source pixel; otherwise, it is a background pixel. So it is natural to consider this as a multiple testing problem with the null hypothesis at each pixel being that $\lambda_{1,ij} = 0$. At a coarse level, we want to characterize the set $\mathcal{S} = \{(i, j) : \lambda_{1,ij} > 0\}$ of source pixels, but our more specific goal is to identify and locate the underlying sources, so that an accurate catalog can be constructed. This requires a more stringent criterion for success because the objects are coherent, localized aggregates. As Figure 1 shows, with the same number

of pixel-wise type I and type II errors, it is possible to get widely varying accuracy in the resulting catalog. Put another way, our loss function operates on the catalog, not the pixels themselves.

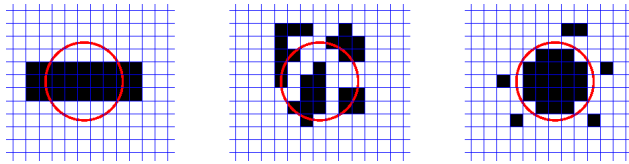


Figure 1: The 45 pixels that have any overlap with the red circle are considered sources and black pixels indicate sources detected via some detection algorithm. Each of the three images have 6 Type I error pixels and 24 Type II error pixels. The detection in the left image captures the center of the source but clearly misses the shape. The detections in the center image show several different sources that have some overlap with the true source. The detection in the right image captures the center of the true source and has some spurious noise detections. While all these pictures have the same number of pixel-wise Type I and Type II errors they lead to very different conclusions about the number, shape and location of the sources in the image, thus a testing criteria based on the aggregate sources, instead of pixels, is necessary.

In this paper, we extend the False Cluster Proportion (FCP) controlling procedures introduced by Perone Pacifico et al. (2004) to make it effective for controlling the rate of false sources detected in astronomical images. As we will show below, the original FCP procedure does not perform well with the Poisson statistics common in the source detection problem and even where the Gaussian assumption holds, does not yield sufficient power to be viable for the astronomical source detection problem. We generalize the technique so that it applies to a wider range of noise models. We also introduce a new transform, which we call the *Multi-scale Derivative*, that enhances sources and significantly improves power. Taken together, these extensions lead to a new procedure that we call the Multi-scale False Cluster Proportion (MSFCP) procedure. This gives a powerful source detection technique that provides rigorous control over the rate of false *sources*, where techniques in current use provide control over the rate of false *pixels*, if they provide any control at all. We demonstrate both the excellent power and error control on a very deep and high resolution telescope image from the Chandra X-Ray Observatory. MSFCP has detection power competitive with the existing procedures, even detecting a source that was overlooked in previous studies while at the same time maintaining rigorous control over the rate of false sources. Although the source detection problem is ubiquitous in Astronomy it also occurs in other settings and we present an example of how FCP concepts can be extended to detecting bands of neural activity in the brain.

Due to its prevalence and difficulty, there have been a variety of approaches to the source detection problem, both in the statistical and astronomical literature. Given the recent explosion in research on multiple testing, there is a plethora of available techniques that can be applied directly to the pixel-wise hypothesis tests to reconstruct \mathcal{S} , including Benjamini and Hochberg (1995)[BH], Benjamini et al. (2006), Storey (2002), Sun and Cai (2007), and Meinshausen and Rice (2006). However, because these methods give error-rates in terms of the individual pixel-wise tests, it is not obvious how to translate these error-rates to make inferences about the underlying sources. Multiple

testing approaches that are less pixel-centered have been developed in the related problem of analyzing functional magnetic resonance imaging (fMRI) data. In this problem, the sources are regions of neural activity that reveal themselves through a measurable change in blood flow response. Worsley et al. (1996) and Worsley et al. (2002) use level sets of a random field formed from test statistics to identify regions containing sources. Heller et al. (2006) construct a test based on clusters instead of pixels in the fMRI setting, but this technique takes advantage of a temporal dimension that is not available in many general (e.g., astronomical) problems.

Source detection understandably garners much attention in the astronomical literature. Astronomers address source detection as one step in a data-processing pipeline – the series of operations performed on the data from collection until catalog. These include, but are not limited to, corrections for atmospheric effects, image registration, filtering out unwanted signals, as well as source detection. These pipelines are typically planned and developed well before the instrument is operational. During the planning stage, simulations are run to test the pipeline including the source detection algorithm (e.g., Sehgal et al., 2007). Astronomers typically do not require their algorithms to satisfy any formal performance criteria; rather, they apply an empirical criterion, using data simulated to look like a real telescope image to calibrate the error rate for detected sources that will be expected in practice. Of course, this depends on the simulated and real data being both quantitatively and qualitatively similar. While great effort and ingenuity are applied in constructing realistic simulations – sometimes years of computing time for a single run – the simulations still rely on untested and unstated assumptions that may fail when the instrument comes on line.

The source detection methods used by astronomers fall into three general classes: simple thresholding, peak-finding algorithms, and Bayesian algorithms. Simple thresholding consists of choosing an intensity cutoff for pixel-wise statistics and classifying any pixel above threshold as a source. It is popular because it is simple and fast, easily computed by the popular SExtractor software (Bertin and Arnouts, 1996). Before thresholding, filters are often applied to the raw data to suppress confounding background signals. In Vikhlinin et al. (1995) and Melin et al. (2006), Matched Filters are used to isolate the signal, and then thresholds are determined using simulated data to create catalogs in X-ray and Radio telescope images respectively. Hopkins et al. (2002) also use simple thresholding, choosing the threshold to control the False Discovery Rate via the method of Benjamini and Hochberg (1995), but they use simulated telescope images to calibrate between rate of false pixels and the rate of false sources.

Peak-finding algorithms search for local maxima in the denoised image and catalog them as sources. Vale and White (2006) and Sehgal et al. (2007) use peak-finding algorithms to look for large galaxy clusters in simulated radio telescope images. The wavelet-based technique of Freeman et al. (2002) is commonly used to detect X-ray sources as in Valtchanov et al. (2001) and Giacconi et al. (2002). Damiani et al. (1997) and Gonzalez-Nuevo et al. (2002) provide a good overview of the popular Mexican Hat wavelet as a tool for source detection. Several implementations exist in software and most are specifically tailored for a certain instrument or type of problem. Pixel-wise error rates for wavelet source detection can sometimes be determined analytically but are more often approximated from simulations. As with simple thresholding, simulations are often used to indirectly estimate the rate of false sources, the error rate of interest, from the rate of false pixels.

Bayesian techniques have become popular with astronomers and several have applied Bayesian methods to source detection as in Savage and Oliver (2007), Strong (2003), and Hobson and McLachlan (2003). Bayesian detection algorithms typically define models for sources, often two-dimensional Gaussians, and attempt to distinguish them from backgrounds via inference on a posterior distribution. Guglielmetti et al. (2009) use Bayesian mixture models to separate sources from background, while Carvalho et al. (2009) propose ways to speed up Bayesian source detection, which can be computationally slow for large problems. Bayesian algorithms typically require more assumptions to be made a priori and can be more computationally expensive than thresholding or peak-finding algorithms.

Our goal in source detection is to detect the relevant objects, not pixels, while controlling the error rates. Statisticians have developed numerous methods for dealing with error rates but have not been focused on detecting aggregate objects, while astronomers have been thinking about detecting objects, but without a rigorous approach to controlling error rates. We propose a technique that does both: control the error rates and make our inference about the sources themselves.

We demonstrate our techniques on an important data set from the Chandra X-ray Observatory, one of the most powerful telescopes in existence. For the Chandra data, our goal is to detect the X-ray sources with a bound on the error rate for sources. We describe an approach due to Perone Pacifico et al. (2004) that gives us a probabilistic bound on the error rate for sources, and apply it to the Chandra data. We find that while this approach gives us the error control we want, it does not have good power when compared to other techniques. We introduce a generalization of the technique that allows for us to keep a probabilistic bound on the error rate for sources under more general conditions. We then introduce a new Multi-scale technique that is designed to enhance sources and thus increase power. We then integrate it with our generalized procedure to get the MSFCP procedure which increases power while maintaining control over the error rate. This improvement is evident when we revisit the Chandra data – we show that our power using MSFCP is competitive to two algorithms commonly used by astronomers, but with superior error control. Furthermore, using our procedure we detect a X-ray source which had gone undetected in the original analysis of the data by astronomers. We then provide a brief description of how these techniques can be used outside the realm of Astronomy with an application to high-resolution neuroimaging data. We conclude with an overview of our results and directions for further study.

2 The Data

We demonstrate our techniques on data from the Chandra X-ray observatory (Weisskopf et al., 2000), one of the most powerful X-ray telescopes in the world. Chandra orbits Earth, at approximately one third the distance to the Moon. Being outside of the Earth’s atmosphere allows for extended observing time without atmospheric disruption of the X-ray signals themselves. X-rays are emitted when matter is heated to millions of degrees, such as in the hot gas surrounding large galaxy clusters, during supernovae, or when matter circles a black hole. Resolving discrete sources of X-rays in space has been an important problem in Astronomy for several decades. Because studying X-ray emissions from galaxy

clusters can answer many of the fundamental questions in Astronomy and Cosmology, several generations of instruments have been developed specifically for this task. From X-ray data, astronomers can infer the evolution of galaxies, which informs us about the evolution of the universe. For instance, recent X-ray observations of the Bullet Cluster have provided the most compelling evidence of dark matter (Markevitch et al., 2004), a mysterious form of matter that does not strongly interact with visible matter but is postulated to account for approximately 22% of the mass of the universe.

The data used in this paper comprise part of the Chandra Deep Field South (CDFS), a composite image of 11 Chandra observations of a small patch of sky with nearly one million seconds of observing time. This is a long exposure which means we should be able to resolve very distant and faint sources. This piece of sky was selected because it had low interference from our own galaxy and no bright stars in its vicinity. The CDFS has area approximately one half the angular size of the moon. It is also in a location that can be observed by several complementary ground-based telescopes. The part of the CDFS that we will analyze and discuss in this paper can be seen in Figure 2. The first step in converting the raw image data into an actionable scientific dataset is cataloging all the sources in the image. The sources in the CDFS are thought to be active galaxies and quasars with massive black holes in their centers. We will provide a new analysis of this dataset that not only detects these important X-ray sources, but also makes a probabilistic guarantee on the rate of falsely detected sources.

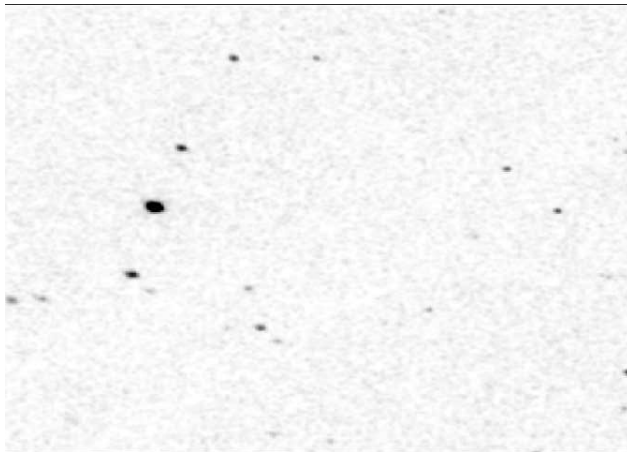


Figure 2: A 512 pixel by 512 pixel patch of the Chandra Deep Field South. The image was smoothed and then all pixels with count greater than 15 were set to 15. This image is the log of that image plus one. The transformations were performed so that the brightest sources do not wash out the fainter ones for display purposes. They were not used in any of the analysis. The complete data set is publicly available from <http://cxc.cfa.harvard.edu/cda/>

The original analysis of the CDFS was published in Giacconi et al. (2002) [GI]. Their main catalog was created by combining the catalogs from two different source detection algorithms: a modified version of the SExtractor algorithm (Bertin and Arnouts, 1996), and the WAVDETECT algorithm (Freeman et al., 2002). The SExtractor algorithm estimates the background and catalogs as a source any region that is 2.4σ above the background that is also at least 5 pixels in area. These parameters are determined using

images simulated to look like the real telescope images. They are selected to create a large catalog which will likely include several false sources. Independently, the WAVDETECT procedure was run using a wavelet transformation specifically tuned for this type of image to detect sources. Again, parameters are calibrated using simulated images. The two catalogs are merged and then refined using follow-up observations in an effort to remove sources that may be false. In this step they are attempting to replicate the detection with independent observations, thus if an object is in the catalog we are fairly certain it is real since it has been observed multiple times, often with a completely different instrument. It is important to note that this detection strategy is designed for a small patch of sky with the ability to follow-up all potential detections. In this scenario, it makes sense to use a detection scheme that casts a wide net. Since we can go back and verify or reject each potential detection we will tolerate a larger number of spurious sources initially in exchange for the ability to detect some fainter sources. This strategy will fail with newer telescopes that will be scanning large areas of sky and making so many detections that it will be impractical to follow-up each and every detection. Instead we want a strategy that will automatically detect real sources reliably while controlling the rate of false ones in one pass through the data.

3 False Cluster Proportion Algorithm

A reasonable first approach for detection is to conduct a hypothesis test at each pixel individually. We want to test whether a pixel is a background pixel (null) or a source pixel (alternative). After conducting the appropriate pixel-wise test, a multiple testing correction can be applied such as the BH method. A problem with the pixel-wise testing approach is that the unit of inference are individual pixels. A pixel is an artificial unit related to the resolution of instrument. What we are interested in are objects composed of collections of adjacent pixels. Therefore, we want the unit of inference to be a cluster as opposed to a pixel. An alternative to pixel-wise testing is the False Cluster Proportion (FCP) procedure introduced by Perone Pacifico et al. (2004). The method is designed to bound the rate of false regions of a random field. FCP treats the image as a realization of an underlying random field and then derives a confidence superset for the location of the true nulls (background regions). Denote the the unknown true nulls as the set S_0 and the confidence superset as U . U is a $1 - \alpha$ confidence superset for S_0 if

$$P(U \supseteq S_0) \geq 1 - \alpha \quad (2)$$

Let L_t denote the level set of all pixels that have intensity greater than t . L_t can be decomposed into its connected components. Every pixel in L_t is grouped with all its neighboring pixels that are also in L_t creating clusters of pixels with intensity greater than t . This decomposition yields a set C_t of k_t clusters $C_t = \{C_{1,t}, C_{2,t}, \dots, C_{k_t,t}\}$. For any cluster C the cluster is declared false if

$$\frac{\lambda(C \cap S_0)}{\lambda(C)} \geq \epsilon \quad (3)$$

In a pixelized image one can use the counting measure and ϵ is a pre-specified tolerance parameter. The goal is to come up with a threshold t that insures the proportion of

detected objects that are false is sufficiently low. Define the true false cluster proportion, $\Xi(t)$:

$$\Xi(t) = \frac{\#\{1 \leq i \leq k_t : \frac{\lambda(C_{it} \cap S_0)}{\lambda(C_{it})} \geq \epsilon\}}{k_t} \quad (4)$$

This quantity can be bounded by calculating the false cluster proportion envelope $\bar{\Xi}(t)$, where

$$\bar{\Xi}(t) = \frac{\#\{1 \leq i \leq k_t : \frac{\lambda(C_{it} \cap U)}{\lambda(C_{it})} \geq \epsilon\}}{k_t} \quad (5)$$

Then from Perone Pacifico et al. (2004)

$$P(\Xi(t) \leq \bar{\Xi}(t) \forall t) \geq 1 - \alpha \quad (6)$$

Suppose we have a confidence superset U , next we need to find the value t_c such that $\bar{\Xi}(t_c) = c$ where c is the false cluster proportion value which we do not wish to exceed. To do this one must perform a search over the possible values of t . Once t_c has been determined, take the k_{t_c} clusters from the level set L_{t_c} as the detected objects. They have the property that with probability $1 - \alpha$ the proportion of the detected objects which are false detections are less than or equal to c .

To use FCP one needs a confidence superset U , which satisfies Equation 2. Perone Pacifico et al. calculate U by looking for the smallest set A for which the null of the following test cannot be rejected.

$$H_0 : A \subset S_0 \text{ versus } H_1 : A \not\subset S_0 \quad (7)$$

In practice, the maximum pixel value in the set A is used as the test statistic. The p-value is then

$$p(x, A) = P_0(\max(Y_{ij} \in A) \geq x) \quad (8)$$

U is calculated by starting with the entire image and then progressively removing the pixels with the highest intensity (those least likely to be part of the background) until the p-value of the remaining set passes α . The p-value in Equation 8 is calculated using the Piterbarg approximation (Piterbarg, 1996). The Piterbarg approximation assumes that the field is a locally stationary Gaussian random field with quadratic covariance. If $X(s)$ is a homogeneous Gaussian random field then $\frac{X}{\sigma}$ is locally stationary with quadratic covariance if for some matrix B ,

$$\rho(s) = 1 - s^T B s + o(\|s\|^2) \quad (9)$$

This method yields a valid confidence superset U for the case of Gaussian Random Fields that satisfy Equation 9, which can then be incorporated into FCP to find the appropriate value for t_c . The clusters detected using the cutoff t_c will, with high probability, have a false cluster rate less than the bound c . Henceforth we will refer to this approach as the PP method; for full details see Perone Pacifico et al. (2004).

Once we have run FCP, astronomers can plug the value t_c as an argument to the SExtractor software and generate the catalog without having to learn any new software

and at computational speed to which they are accustomed. Many astronomers use SExtractor for source detection either using the default settings or by “playing with various parameter combinations and inspecting the results by eye” (Shim et al., 2006). FCP gives astronomers a more principled way to choose the parameters in the software they are already using.

4 FCP Applied to CDFS

In the CDFS data, the objects we are looking for are active galaxies and quasars which are emitting X-rays. We would like to detect as many of these objects as possible without making spurious detections, that is classifying what is really just noise as an X-ray emitting object. Each pixel records the number of photons that strike the detector and are modeled as Poisson random variables. The mean background in these images is small, approximately 0.3, which violates the assumption of the PP procedure which assumes a Gaussian background. Our initial approach to dealing with the non-gaussianity is to filter the data so that the Gaussianity assumption is more appropriate. Specifically, we first smooth the data and then apply a pixel-wise transformation. Smoothing the data with a Gaussian filter effectively aggregates counts so we preserve most of the structure of the Poisson data even though they are no longer counts. There are also many more unique values which makes it closer to high rate Poisson data than low rate Poisson data, which is mostly zeros and ones. We then take the square root transformation which makes the background approximately Normal. The square root transformation has been shown to normalize high count Poisson data (Anscombe, 1948). Using simulations, we have tested the effectiveness of our smooth-then-square-root procedure for low rate Poisson data and found that for rates as low as 0.2, it yields approximately normal data. Examples for different rate parameters is shown in Figure 3.

After the normalizing transformation, we perform a standard Z-test at each pixel, assuming a constant background mean, and calculate the 95% confidence superset for the background by applying the PP method to the test statistics. We then run FCP on the test statistics as described in Section 2, bounding the rate of false sources to be less than 10%. Because our U is very conservative (it contains every pixel from the null with probability .95) we select $\epsilon = .99$ to maximize our detection power. Nothing in our procedure relies on information about the telescope or knowing the nature or distribution of the sources themselves. We only assume that our normalizing transformation does indeed give us a background that is approximately Gaussian, an assumption which can easily be checked. FCP, using the PP method to calculate U , detects 17 sources, all of which are in the previously published GI catalog as seen in Figure 4. Since this catalog has been verified with follow up observations we believe all the detections are real. However, this analysis is clearly missing many clusters that should be detectable – nine of the 26 clusters in the Main catalog of GI were missed using FCP with the PP method.

One way to boost the power is to run the data through an appropriate filter that will enhance the sources and help separate them from the background. However, to do that and maintain the desired control over the rate of false sources, we need to adapt FCP so that it can handle more varied noise conditions. This means moving away from the PP method to a more general procedure for calculating U . In the following section we

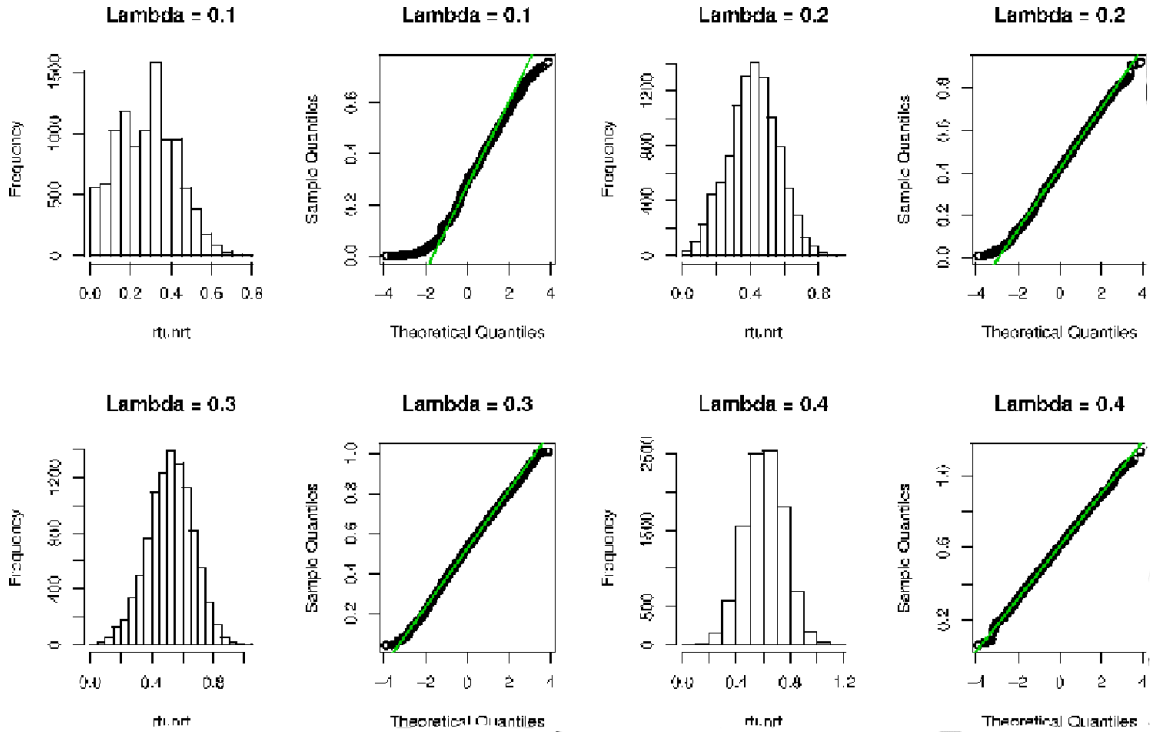


Figure 3: Simulation of a 100×100 image of Poisson Background which is then smoothed with a Gaussian, with standard deviation of 1 pixel. The square root is then taken at each pixel. The histogram shows the pixels become approximately normal for values of lambda above .2. The Quantile-Quantile plots show the data compared to a perfectly normal distribution. The closer the points lie to the line $y=x$ (green), the closer the data is to a normal distribution

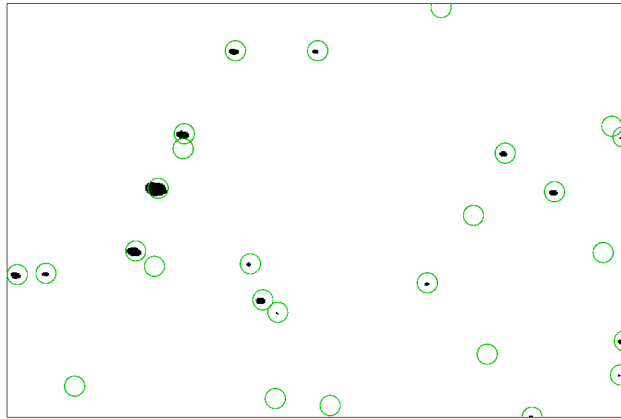


Figure 4: CDFS data after applying the False Cluster Proportion procedure using the PP method to calculate U . Black indicates sources detected by FCP and the circles are detections from both the Main Catalog and Secondary Catalogs from GI. There are 17 detections from FCP all of which are in the Catalog and 9 missed sources.

propose a procedure for calculating U under any noise distribution that we can simulate. This will allow us to run FCP on filtered data and achieve higher power while maintaining

control over the rate of false sources.

5 Generalizing FCP

The False Cluster Proportion Algorithm requires the derivation of a confidence superset for the background of an image. What we have been referring to as the PP method, which is based on the Piterbarg approximation, is limited to cases where test statistics are or can be transformed to a Gaussian Random Field that satisfies Equation 9. But in many situations the data are not Gaussian and finding an acceptable transformation is infeasible. For example, filtering techniques commonly used to enhance sources will usually not satisfy the assumptions of the PP method.

To broaden the scope of the technique, we have developed a simulation procedure that produces an accurate $1 - \alpha$ confidence superset for any noise distribution from which we can sample numerically. Assume our data are a rectangular image with N total pixels and known noise distribution F . We simulate noise images and calculate the maxima of subsets of the images. We build up empirical distributions for these maxima and use them to calculate the p-values which, in the PP method, were calculated using the Piterbarg approximation. We can then plug the p-values into the FCP procedure and get the False Cluster Proportion guarantee (Equation 6), for a much wider variety of noise conditions than the PP method.

Algorithm 1:

For each $b \in \{1, \dots, B\}$

1. Simulate an image, Y^b , with the same dimensions as the data, with noise distribution F and no sources
2. Record the maximum value of the image, $Y_{(N)}^b$
3. For $k = 1, 2, \dots, a$ randomly remove k pixels and record the maximum remaining pixel value $Y_{(N-k)}^b$. $N - a$ is the smallest number of pixels for which you want to calculate the p-value, it needs to be more than the number of pixels that you believe to be sources, but the number of computations increase with a

In this way, we build the distribution of the maximum for a given area under the null. Then we can calculate the appropriate p-values

$$p(x, A) = P_0(\max(Y_{ij} \in A) \geq x) \quad (10)$$

which were previously approximated using Piterbarg's formula and are now estimated using the simulated data

$$p(x, A) \approx \frac{\#\{1 \leq i \leq B : Y_{(\text{Area}(A))}^i \geq x\}}{B} \quad (11)$$

Then we proceed as in Perone Pacifico et al. (2004) to calculate U .

For a Gaussian Random Field that satisfies Equation 9 we can compare the Piterbarg formula to our simulated p-values. In Figure 5 we simulate the p-values for different sized

areas A , as described above and also by replacing Step 3 with removing a square region of area A from the image. We see that the p-value from Piterbarg, which accounts for size but not shape, tends to fall in between these two but the differences are small and get smaller as the area gets bigger. For astronomical source detection, the random sampling approach is closest to the data we observe so we use it as our default. However, it is worth noting that our simulation technique is easily adaptable to handle prior knowledge about the shapes of the objects of interest. In addition, unlike Piterbarg, our simulation procedure gives accurate p-values for any x , not just those in the tail. However, the biggest benefit of simulating the p-values is we are not restricted to smooth Gaussian Random Fields and instead can handle a wider range of noise conditions.

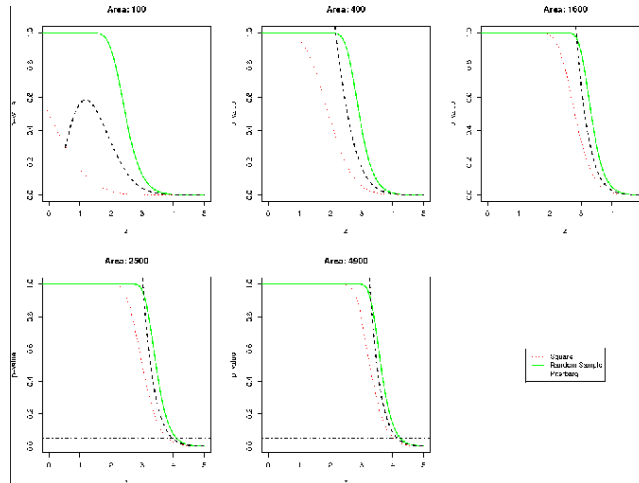


Figure 5: P-values for a Gaussian Random field that satisfies Equation 9 for different sized regions. The dotted black line is the value from Piterbarg that does not consider any shape information, the solid green line is calculated using a simulation that randomly samples regions of area 1, the dotted red line is using the same simulation but the area used is from a square region. Shape information appears to have a mild effect that gets smaller as the area considered gets larger. Also Piterbarg exhibits strange behavior for small areas. The simulation was run 10,000 times.

We can simplify the simulations further. We note that $P(x, A) > P(x, A - k) \forall k > 0$. Since we are dealing with large images, where the source signal is sparse relative to the background, the maximum over N pixels is not going to be substantially different than the maximum over $N-k$ pixels when $N \gg k$. Thus if we use the following algorithm we will get a comparable confidence superset directly and with less computation.

Algorithm 2:

1. For each $b \in \{1, \dots, B\}$, simulate an image, Y^b , with the same dimensions as the data, with noise distribution F and no sources, then record its maximum
2. Calculate $r_{1-\alpha}$, the $1 - \alpha$ percentile of the maxima
3. Using the original data image, calculate the level set $U = (L_{r_{1-\alpha}})^C$

Then U is a $1 - \alpha$ confidence superset for the null. Using the second algorithm is faster because we avoid the computation of the aB maxima at the cost of having a bigger confidence superset U . However as long as $N \gg k$, which will be the case for telescope images where sources are relatively sparse on the sky, the size difference is negligible. The second algorithm also allows us to calculate U directly without having to search over sets or approximate any p-values.

These simulations are only meant to approximate a confidence superset for a given null distribution – it is not meant to simulate the complex systems in the real data. Therefore we do not need to use prior knowledge or make assumptions about the underlying Astronomy as in the simulations commonly used by astronomers for source detection. Our simulated confidence superset U can be calculated for any noise condition from which we can sample numerically. Furthermore we can also simulate what happens if we apply filters to the data as is commonly performed in astronomy. Filters can often be used to enhance sources and remove background contamination, making detection easier. For instance if we know our data have a Poisson noise distribution, we can simulate the Poisson noise image, apply the filter, and then calculate the maxima of the filtered image. We then can calculate the confidence superset for filtered Poisson data. This combination of filtering and false cluster proportion control will give us a very powerful tool for source detection.

6 Using Multi-scale Derivatives to Enhance Detection Power

We have seen with the Chandra data that FCP, using a Z-test and the PP method, does not achieve power comparable to the methods in Giacconi et al. (2002)[GI]. In the previous section, we outlined a simulation-based approach which replaces the PP method, allowing for more general test statistics that do not necessarily have to be Gaussian. In this section, we describe a new technique which directly address two problems contributing to the lack of power seen in Section 4. The first problem is that the Z-test assumes a constant background mean. While this is often a reasonable assumption, there may be locations in the image where this does not hold; for example at the edge of exposures where certain pixels may have been exposed longer than others. In general, telescope images can have non-constant backgrounds that vary spatially, in which case the constant background mean is clearly violated. The second problem is that rules based on the magnitude of a pixel, like the Z-test, are not necessarily the best at discriminating sources from background. To address both of these problems we have developed a Multi-scale Derivative approach which uses local information to identify regions that stand out from the background as sources.

The idea behind Multi-scale Derivatives is to apply a Gaussian filter to the data using a range of bandwidths and examine the derivative of the filtered image with respect to the bandwidth. To get an idea of why this works, we examine a toy example as shown in Figure 6. Suppose we are at a location with no signal. At small bandwidths, our smooth estimate of the null location remains low, and this will stay roughly the same until we reach a bandwidth that is big enough to hit a source, at which point our smoothed estimate will jump up as the source gets smoothed into the null space. The bandwidth

at which this jump occurs tells us how close we are to a source. Alternatively, if we are at a source, we will have a high value for our smooth estimate if our bandwidth is small and as we increase the bandwidth, our estimate will get lower and lower as null areas are smoothed into the source.

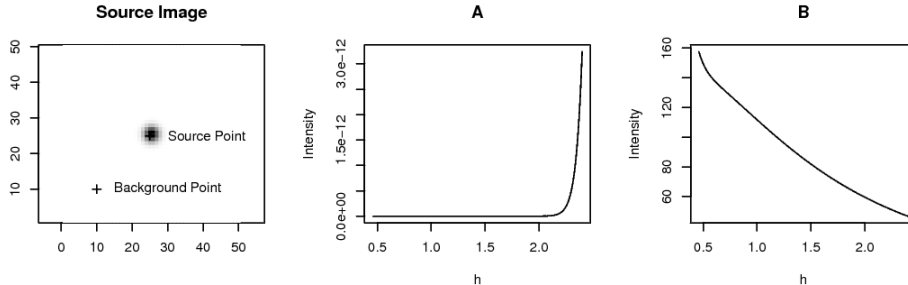


Figure 6: Left: A toy source with a background and a source point highlighted. A: The intensity of the background point after smoothing with different values of the smoothing parameter h . The intensity stays constant around zero until the source begins to get smoothed into the background, at which point we see a small increase in the intensity. B: The intensity of a point in the source after smoothing with different values of the smoothing parameter h . The intensity drops sharply for small amounts of smoothing and continues to decline for larger values of h . Thus estimates of the derivative of the source point with respect to h should give large negative values whereas the background point will not.

If we compare the derivative of our smoother with respect to the bandwidth, sources will stand out by their large negative derivatives. The smoothing operation can be calculated quickly by performing the convolution in Fourier space, and we can use the same trick to calculate the required derivative of the smoother. The derivative is calculated by convolving the data with a filter of the form

$$F_h(u, v) \propto \left(\frac{d(u, v)^2}{h^3} - \frac{2}{h} \right) * \phi(u, v|h) \quad (12)$$

where $d(u, v)$ is the distance between the origin and point (u, v) . ϕ is a symmetric Gaussian kernel with bandwidth h . We then choose a value for h and convolve the filter with the image to get an image which estimates the derivative for each pixel at the scale h . We do this for a few values of h which are selected to cover the range of source sizes. The Multi-scale Derivative image, M , is then created at each pixel by selecting the minimum derivative at that pixel over all the scales.

$$M(u, v) = \min_h F_h(u, v) \quad (13)$$

As a result, we should see high negative values at the location of sources in M . The Multi-scale Derivative image M measures the peakedness in the data caused by sources in cases where the background is smoothly varying and will enhance sources in images where there is a flat background. As a demonstration, in Figure 7 we show a small dataset due to Sehgal et al. (2007) simulated to look like data from the Atacama Cosmology Telescope

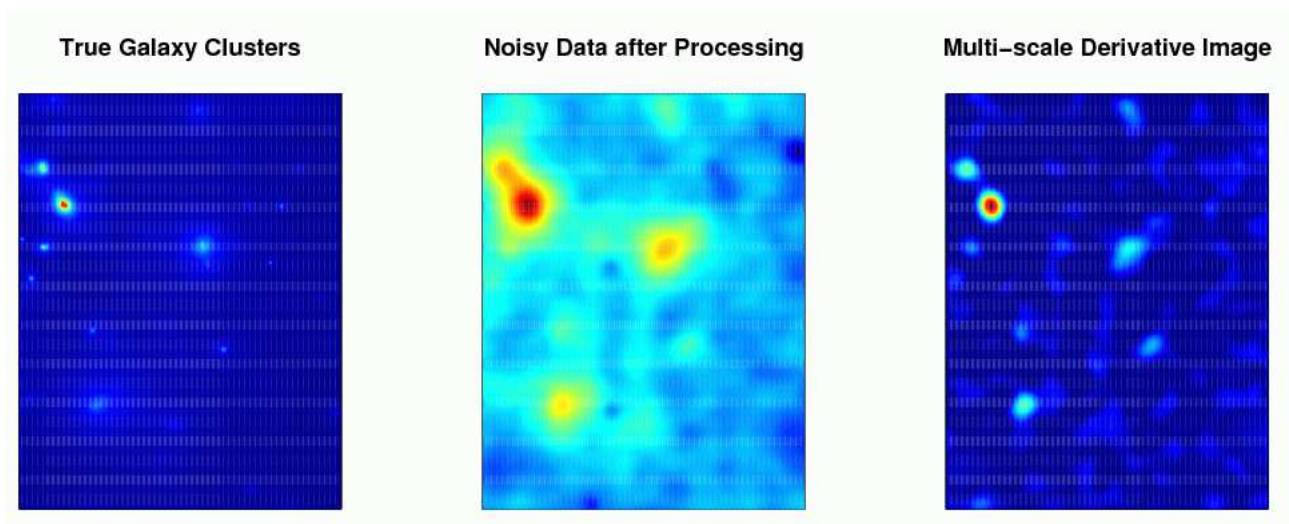


Figure 7: Left: The galaxy clusters we want to detect. In practice these will be obscured by confounding radio signals Middle: The Wiener filtered image which combines information from three different frequencies in an attempt to pick out the signal from the galaxy clusters while eliminating the confounding signals. This filter has introduced a non-constant background to the image Right: The Multi-scale Derivative image calculated from the Wiener filtered image recovers most of the sources we are trying to detect while getting rid of most of the background variation. Data courtesy of Sehgal et al. (2007)

(Kosowsky, 2003), a ground-based radio telescope used to detect large galaxy clusters. The clusters we wish to detect are visible as bright spots in the simulated image on the left. In practice, we cannot observe these clusters directly because they are obscured by several other stronger radio sources. To isolate the clusters, Sehgal et al. use a Wiener filter, which combines data from three different radio frequencies, as seen in the middle image. Our goal is to detect the galaxy clusters from the filtered image. The brightest sources are visible in the Wiener filtered image, but the background is spatially varying and is much brighter in certain areas than in others. Any detection algorithm based on the magnitude of pixels will not perform well on this image. Instead we calculate the Multi-scale Derivative image from the filtered image as seen in the right panel of Figure 7. The Multi-scale Derivative image suppresses the background and highlights the sources, which will make source detection much easier. In this example, the Multi-scale Derivative is used as a filter which enhances sources in the image while suppressing background. Alternatively, it can be viewed as a test-statistic which incorporates local information to test for peaks in the data. Multi-scale Derivatives can be combined with the simulation procedure described in Section 5 to create a catalog with False Cluster Proportion control, the MSFCP procedure. We expect that the catalog created this way, which is specifically designed to draw out sources, will give us more detection power than using a simple Z -test statistic.

7 MSFCP on Chandra Data

We expect that using the Multi-scale Derivative filter on the CDFS image will enhance the clusters, making them stand out more from the background. After performing the smooth-then-root transformation as described previously, we compute the Multi-scale Derivative image. We then ran FCP on the Multi-scale Derivative image M , using a confidence superset that was obtained using Algorithm 2 as outlined in Section 5. We will refer to this procedure as the MSFCP procedure. Using MSFCP with the same parameters as before we detect 24 of the 26 sources detected in the main catalog. We do not make any detections outside of the catalog. Since the detections in the catalog have been replicated in follow-up observations this suggests that we are not making any false detections while still detecting almost all of the real objects.

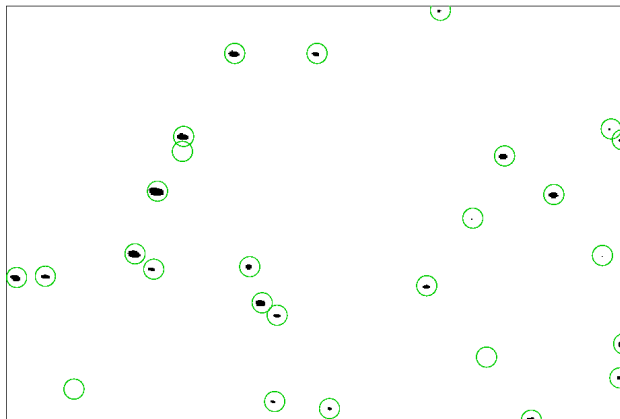


Figure 8: CDFS data after applying MSFCP procedure. Black indicates sources detected by FCP and the circles are detections in both the Main Catalog and the Secondary Catalogs from GI

Without having to simulate images made to look like the telescope images, make any assumptions about the underlying astronomy, and without conducting follow-up observations, we can still make the statement that with probability .95 less than 10% of our detections will be false. The other algorithms cannot make such an explicit guarantee of a pure sample.

The detection strategy used in Giacconi et al. (2002), which we refer to as GI, is designed for a small patch of sky with the ability to follow-up all potential detections. In this scenario, it makes sense to use a detection scheme that casts a wide net. Because we can go back and verify or reject each potential detection we will tolerate a larger number of spurious sources initially in exchange for the ability to detect some fainter sources. This wide net strategy is unfair to our MSFCP approach which was run to keep the false detection rate less than 10% without the benefit of additional data. To mimic this wide net approach we can relax our parameters. If we allow for the proportion of false sources to grow to 20% we detect 26 sources, two of which are new detections outside of the main catalog. We do not have the resources to follow up both of these new detections, however one of the new detections is close to two detections in the published catalog. This allows us to look at the follow-up optical observation for that area to verify our new detection.

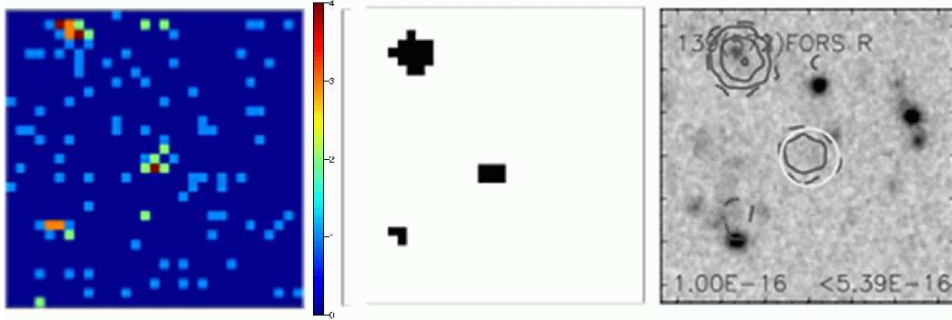


Figure 9: Left: Raw photon counts from the telescope. Center: Black regions are the three sources detected by MSFCP using a tolerance of 20%. The detection in the middle and upper left are also detected and verified in GI. Left: The optical counterpart observation for the source in the center from Giacconi et al. (2002). The contour lines indicate X-ray activity at 3,5,10, and 20 σ above the local background. We can clearly see a source that overlaps with our detection in the lower left, suggesting it is not a spurious detection.

In Figure 9, we show the original X-ray photon counts for the region. Visually we see three candidates and using a False Cluster Proportion tolerance of 20% we detect all three. In the final panel of Figure 9 we see the optical follow up which clearly shows an object at the location of our new detection. Thus we are confident that this new detection is in fact a real source that was missed by the analysis in GI. Our procedure has not only captured almost all of the detections from the previous analysis but with rigorous error control, it has also found a new source that was missed by the astronomers.

Comparison of Detection Procedures			
Method	False Cluster Proportion Tolerance (c)	% of Main Catalog in GI recovered	# of New Verified Detections outside of GI
PP	10%	65.3%	0
MSFCP	10%	92.3%	0
MSFCP	20%	92.3%	1

We do not have corresponding optical data for our other detection so we are unable to verify whether it is a real detection or not. If it is real we would have no spurious detections while making two new detections. Even if it is not real we would still have an error rate of 3.8% which is well under the 20% we are willing to accept. We expect the proportion of false sources one is willing to tolerate to be a parameter that astronomers will have to determine to suit the problem at hand. For instance, the “wide-net” approach works adequately for small data sets, but newer telescopes, like LSST, will collect such a large amount of data that following up each potential detection is impractical. In this scenario having a detection procedure that controls for the proportion of false detection automatically in one pass will be vitally important.

8 Beyond Astronomy: An illustration for other types of objects

To illustrate the reach of our method, we apply it to data from a fMRI experiment. We do not aim here to provide a definitive analysis of these data, but rather to show how our method can be adapted beyond astronomical images. We will report on a full analysis of these data in another paper.

In a functional Magnetic Resonance Imaging experiment, a participant is placed in the Magnetic Resonance scanner and asked to perform a carefully arranged sequence of behavioral tasks while three-dimensional brain images are acquired at regular intervals. Concentrated neural activity produced by performing the tasks induces detectable but subtle changes in the images due to a blood-flow response in the brain. A common form of analysis for fMRI data considers the time series of measurements at each location in the image and computes a statistic for that location that is designed to detect task-related changes in the signal. “Hot spots” in images of these statistics roughly correspond to areas of activity in the brain. See Genovese (2000) for more detail on this process.

Here we consider a simple experiment in which the participant is asked to visually fixate on a spot at the center of the visual field while two complementary sets of annular rings flash alternately at a fixed frequency. The images were acquired using a new technique that provides much higher spatial resolution than is typical for fMRI studies without sacrificing temporal resolution. The three-dimensional images are then projected down to the two-dimensional surface of the brain. We thank Drs. David Heeger and Eli Merriam at NYU for the use of these data.

At each location in the primary area responsible for visual processing (called V1), the fMRI signal should vary roughly like a sinusoid, as the corresponding location in the visual field turns on and off. Locations that respond to the first set of rings should have sinusoidal signals 180° out of phase to locations that respond to the second set of rings.

Our goal is to identify the regions in V1 that activate in response to each set of stimuli. This will appear as a series of bands across the visual cortex with alternating bands out of phase with each other. As in the astronomical problems, we are interested in the active regions themselves rather than the individual pixels, so we prefer an inferential method that can give us control over regions as opposed to pixels.

To detect the periodicity at each location, we use a variant of Fisher’s F -test (Brockwell and Davis, 1993) for each time series to determine if that location is responsive to the stimulus. For each location, we also have the response phase which, for locations that respond to the stimulus, we expect to cluster corresponding to the differing sets of rings. This leaves us with three basic types of locations which we want to differentiate, null locations for which there is no response to the stimulus, locations that respond to the first set of rings and those that respond to the second set of rings. We run a simple classifier on the phases to partition the locations into two phase classes which correspond to the two different stimulus rings. We then want to conduct a test that will group locations into clusters corresponding to the phases with a probabilistic guarantee on the rate of false clusters. To do this we need to adapt our definition of a cluster to both deal with having multiple classes of clusters and also to dealing with points in space as opposed to pixels on a regular grid. For multiple classes of clusters we first have to classify each location into a class and then we modify our definition of a cluster such that a cluster must be made up

of locations all belonging to the same class.

To handle the points in space, we define a graph on the points. We call two locations connected at level t if they are both of the same class, have p-values from the F-test less than t and there is a path between the two locations in which each node is also of the same class, has p-values less than t and no edge has euclidean distance greater than d . Then the i th connected component at level t , $C_{i,t}$, is the largest set of locations that are all connected.

We also need to derive a confidence superset U . Recall, U is a $1 - \alpha$ confidence superset for S_0 if $P(U \supseteq S_0) \geq 1 - \alpha$. Our null has already been determined by the F-test and for each location we have the p-value of that test. A simple way to calculate U is to find the $(1 - \alpha)$ th percentile of the distribution of the maximum of the p-values, which will have a uniform distribution under the null. All locations with p-value greater than $1 - (1 - \alpha)^{\frac{1}{n}}$ belong to the set U , where n is the total number of locations. This will provide a conservative confidence superset and future work will use local information to obtain a smaller confidence superset. Now we can proceed similar to the previous cases. For different values of t we examine the connected components and if the fraction of location in $C_{i,t}$ that are also in U is greater than ϵ we declare the cluster $C_{i,t}$ false. We proceed analogous to the case of a pixelized image, searching for the value of t such that the rate of false regions is bounded appropriately with high probability. Figure 10 shows the result of an experiment in which we set our detection limit so that with probability .95 less than 10% of the clusters detected are false. We can clearly see the bands that we are hoping to detect as well as some active areas along the edges which may be artifacts of the projection from three dimensions to the surface of the brain. This is a demonstration that False Cluster Proportion concepts can be extended to various situations where controlling the rate of falsely detected regions is desirable to detect structure. Here we have shown that we can get the same false cluster proportion control when there is more than one class of objects and also when our data do not lie a regular grid.

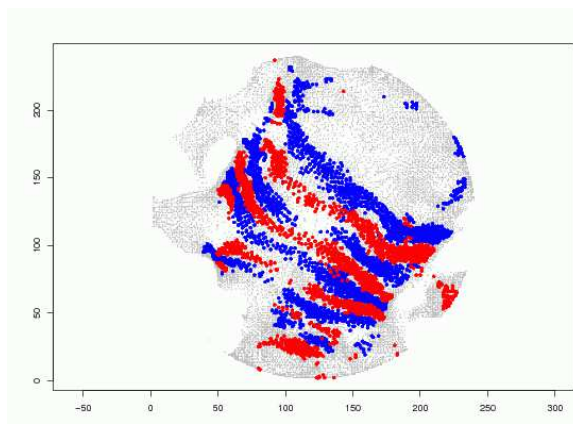


Figure 10: Gray dots represent every location recorded while blue and red dots indicate locations in clusters that were declared active. The two colors denote the two different phases, one corresponding to the rings and the other to the anti-rings. We clearly see the banded activation patterns expected in the data.

9 Conclusion

We have extended the False Cluster Proportion Multiple Testing Procedure so it can now be applied to a wide variety of problem in Astronomy as well as other fields. By moving away from theoretical approximations, like Piterbarg’s approximation, we can now calculate confidence supersets for a large variety of noise conditions. This allows us to create source catalogs with a probabilistic guarantee that they are not overly polluted with false detections without having to make any difficult to check assumptions about the data or the science behind the data. The Multi-scale Derivative procedure enhances the types of sources we typically see in a telescope image and we have shown that they can also enhance the power of False Cluster Proportion source detection algorithms. This is evidenced by our analysis of the CDFS data. The catalog published in GI uses two different algorithms and then has to follow up each detection, whereas we run MSFCP and can make the statement that with probability .95 less than 10% of our detections are false, and still get virtually the same catalog. When we allow 20% of our detections to be false we make two new detections, one of which we have verified is a real source that was missed in the original analysis. Our procedure provides rigorous error control, which is lacking in the current techniques used by astronomers. At the same time we have demonstrated that the detection power is comparable and in fact we have detected sources that they have missed. Controlling false detections without the need for expensive follow up observations will be critical as the next generation of telescopes will provide a deluge of data that will be impossible to process manually.

We have also shown that these ideas can be generalized to other types of problems where we are dealing with points spread along a plane instead of a regular grid of pixels in an image. We can further modify our definition of cluster to differentiate between different types of objects. We can then control the proportion of false clusters, allowing for different classes of clusters. In the future, we believe we can further extend our framework so that we can apply False Cluster Proportion techniques on a wide variety of statistical clustering problems, in which we are trying to detect clusters of data without making false detections.

References

- Anscombe, F. (1948), “The transformation of Poisson, binomial and negative-binomial data,” *Biometrika*, 35, 246–254.
- Benjamini, Y. and Hochberg, Y. (1995), “Controlling the False Discovery Rate: a Practical and Powerful Approach to Multiple Testing,” *Journal of the Royal Statistic Society*, B, 289–300.
- Benjamini, Y., Krieger, A. M., and Yekutieli, D. (2006), “Adaptive Linear Step-Up Procedures that control the False Discovery Rate,” *Biometrika*, 93, 491–507.
- Bertin, E. and Arnouts, S. (1996), “SExtractor: Software for source extraction.” *A&AS*, 117, 393–404.
- Brockwell, P. J. and Davis, R. A. (1998), *Time Series: Theory and Methods (Springer Series in Statistics)*, Springer.
- Buckner, R. L. (1998), “Event-related fMRI and the hemodynamic response,” *Human Brain Mapping*, 6, 373–377.
- Carvalho, P., Rocha, G., and Hobson, M. P. (2009), “A fast Bayesian approach to discrete object detection in astronomical data sets - PowellSnakes I,” *MNRAS*, 393, 681–702.
- Cash, W. (1979), “Parameter estimation in astronomy through application of the likelihood ratio,” *ApJ*, 228, 939–947.
- Damiani, F., Maggio, A., Micela, G., and Sciortino, S. (1997), “A Method Based on Wavelet Transforms for Source Detection in Photon-counting Detector Images. I. Theory and General Properties,” *The Astrophysical Journal*, 483, 350–369.
- Freeman, P. E., Kashyap, V., Rosner, R., and Lamb, D. Q. (2002), “A Wavelet-Based Algorithm for the Spatial Analysis of Poisson Data,” *The Astrophysical Journal Supplement Series*, 138, 185–218.
- Genovese, C. R. (2000), “A Bayesian Time-Course Model for Functional Magnetic Resonance Imaging Data,” *Journal of the American Statistical Association*, 95, 691–703.
- Genovese, C. R., Miller, C. J., Nichol, R. C., Arjunwadkar, M., and Wasserman, L. (2004), “Nonparametric Inference for the Cosmic Microwave Background,” *Statistical Science*, 19, 308–321.

- Giacconi, R., Zirm, A., Wang, J., Rosati, P., Nonino, M., Tozzi, P., Gilli, R., Mainieri, V., Hasinger, G., Kewley, L., Bergeron, J., Borgani, S., Gilmozzi, R., Grogin, N., Koekemoer, A., Schreier, E., Zheng, W., and Norman, C. (2002), “Chandra Deep Field South: The 1 Ms Catalog,” *The Astrophysical Journal Supplement Series*, 139, 369–410.
- Gonzalez-Nuevo, J., Argueso, F., Lopez-Caniego, M., Toffolatti, L., Sanz, J. L., Vielva, P., and Herranz, D. (2006), “The Mexican Hat Wavelet Family. Application to point source detection in CMB maps,” *MON.NOT.ROY.ASTRON.SOC.*, 369, 1603.
- Guglielmetti, F., Fischer, R., and Dose, V. (2009), “Background-source separation in astronomical images with Bayesian probability theory - I. The method,” *MNRAS*, 396, 165–190.
- Heller, R., Stanley, D., Yekutieli, D., Rubin, N., and Benjamini, Y. (2006), “Cluster-based analysis of fMRI data.” *Neuroimage*, 33, 599–608.
- Herschel, W. (1786), “Catalogue of One Thousand New Nebulae and Clusters of Stars. By William Herschel, LL.D. F. R. S.” *Royal Society of London Philosophical Transactions Series I*, 76, 457–499.
- Hobson, M. P. and McLachlan, C. (2003), “A Bayesian approach to discrete object detection in astronomical data sets,” *MNRAS*, 338, 765–784.
- Hopkins, A. M., Miller, C. J., Connolly, A. J., Genovese, C., Nichol, R. C., and Wasserman, L. (2002), “A New Source Detection Algorithm Using the False-Discovery Rate,” *AJ*, 123, 1086–1094.
- Kosowsky, A. (2003), “The Atacama Cosmology Telescope,” *New Astronomy Reviews*, 47, 939.
- Loredo, T. J. (2007), “Analyzing Data from Astronomical Surveys: Issues and Directions,” in *Statistical Challenges in Modern Astronomy IV*, eds. Babu, G. J. and Feigelson, E. D., vol. 371 of *Astronomical Society of the Pacific Conference Series*, pp. 121–+.
- Markevitch, M., Gonzalez, A. H., Clowe, D., Vikhlinin, A., Forman, W., Jones, C., Murray, S., and Tucker, W. (2004), “Direct Constraints on the Dark Matter Self-Interaction Cross Section from the Merging Galaxy Cluster 1E 0657-56,” *ApJ*, 606, 819–824.
- Meinshausen, N. and Rice, J. (2006), “Estimating the proportion of false null hypotheses among a large number of independently tested hypotheses,” *Ann. Statist.*, 34, 373–393.
- Melin, J.-B., Bartlett, J. G., and Delabrouille, J. (2006), “Catalog extraction in SZ cluster surveys: a matched filter approach,” *A&A*, 459, 341–352.
- Perone Pacifico, M., Genovese, C., Verdini, I., and Wasserman, L. (2004), “False Discovery Control for Random Fields,” *Journal of the American Statistical Association*, 99, 1002–1014.
- Piterbarg, V. (1996), *Asymptotic Methods in the theory of Gaussian processes and fields*, American Mathematical Society.
- Richards, J. A. and Jia, X. (1999), *Remote Sensing Digital Image Analysis: An Introduction*, Secaucus, NJ, USA: Springer-Verlag New York, Inc.
- Richards, J. W., Freeman, P. E., Lee, A. B., and Schafer, C. M. (2009), “Exploiting Low-Dimensional Structure in Astronomical Spectra,” *ApJ*, 691, 32–42.
- Savage, R. S. and Oliver, S. (2007), “Bayesian Methods of Astronomical Source Extraction,” *ApJ*, 661, 1339–1346.
- Sehgal, N., Trac, H., Huffenberger, K., and Bode, P. (2007), “Microwave Sky Simulations and Projections for Galaxy Cluster Detection with the Atacama Cosmology Telescope,” *The Astrophysical Journal*, 664, 149–161.
- Shim, H., Im, M., Pak, S., Choi, P., Fadda, D., Helou, G., and Storrie-Lombardi, L. (2006), “Deep u*- and g-Band Imaging of the Spitzer Space Telescope First Look Survey Field: Observations and Source Catalogs,” *The Astrophysical Journal Supplement Series*, 164, 435–449.
- Storey, J. D. (2002), “A Direct Approach to False Discovery Rates,” *Journal of the Royal Statistical Society. Series B (Statistical Methodology)*, 64, 479–498.
- Strong, A. W. (2003), “Maximum Entropy imaging with INTEGRAL/SPI data,” *A&A*, 411, L127–L129.
- Sun, W. and Cai, T. T. (2007), “Oracle and Adaptive Compound Decision Rules for False Discovery Rate Control,” *Journal of the American Statistical Association*, 102, 901–912.
- Tyson, J. A. and the LSST Collaboration (2002), “Large Synoptic Survey Telescope: Overview,” *PROC.SPIE INT.SOC.OPT.ENG.*, 4836, 10.
- Vale, C. and White, M. (2006), “Finding Clusters in SZ Surveys,” *NEW ASTRON.*, 11, 207.
- Valtchanov, I., Pierre, M., and Gastaud, R. (2001), “Comparison of source detection procedures for XMM-Newton images,” *A&A*, 370, 689–706.
- van Dyk, D. A., DeGennaro, S., Stein, N., Jefferys, W. H., and von Hippel, T. (2009), “Statistical analysis of stellar evolution,” *ANNALS OF APPLIED STATISTICS*, 3, 117.
- Vikhlinin, A., Forman, W., Jones, C., and Murray, S. (1995), “Matched Filter Source Detection Applied to the ROSAT PSPC and the Determination of the Number-Flux Relation,” *ApJ*, 451, 542–+.
- Weisskopf, M., Tananbaum, H., van Speybroeck, L., and O’dell, S. (2000), “Chandra X-Ray Observatory: Overview, X-Ray Optics, Instruments, and Missions,” *Proc. SPIE*, 4012.
- Worsley, K., Liao, J., Aston, C., Petre, V., Duncan, G., Morales, F., and Evans, A. (2002), “A General Statistical Analysis for fMRI data,” *NeuroImage*, 15, 1–15.
- Worsley, K., Marrett, S., Vandal, A., Friston, K., and Evans, A. (1996), “A Unified Statistical Approach for Determining Significant Statistical Signals in Image of Cerebral Activation,” *Human Brain Mapping*, 4, 58–73.
- York, D. G., Adelman, J., Anderson, J. E., Jr., Anderson, S. F., Annis, J., Bahcall, N. A., Bakken, J. A., Barkhouser, R., Bastian, S., Berman, E., Boroski, W. N., Bracker, S., Briegel, C., Briggs, J. W., Brinkmann, J., Brunner, R., Burles, S., Carey, L., Carr, M. A., Castander, F. J., Chen, B., Colestock, P. L., Connolly, A. J., Crocker, J. H., Csabai, I., Czarapata, P. C., Davis, J. E., Doi, M., Dombeck, T., Eisenstein, D., Ellman, N., Elms, B. R., Evans, M. L., Fan, X., Federwitz, G. R., Fiscelli, L., Friedman, S., Frieman, J. A., Fukugita, M., Gillespie, B., Gunn, J. E., Gurbani, V. K., de Haas, E., Haldeman, M., Harris, F. H., Hayes, J., Heckman, T. M., Hennessy, G. S., Hindsley, R. B., Holm, S., Holmgren, D. J., hao Huang, C., Hull, C., Husby, D., Ichikawa, S.-I., Ivezić, Z., Kent, S., Kim, R. S. J., Kinney, E., Klaene, M., Kleinman, A. N., Kleinman, S., Knapp, G. R., Korienek, J., Kron, R. G., Kunszt, P. Z., Lamb, D. Q., Lee, B., Leger, R. F., Limmongkol, S., Lindenmeyer, C., Long, D. C., Loomis, C., Loveday, J., Lucinio, R., Lupton, R. H., MacKinnon, B., Mannery, E. J., Mantsch, P. M., Margon, B., McGehee, P., McKay, T. A., Meiksin, A.,

Merelli, A., Monet, D. G., Munn, J. A., Narayanan, V. K., Nash, T., Neilsen, E., Neswold, R., Newberg, H. J., Nichol, R. C., Nicinski, T., Nonino, M., Okada, N., Okamura, S., Ostriker, J. P., Owen, R., Pauls, A. G., Peoples, J., Peterson, R. L., Petravick, D., Pier, J. R., Pope, A., Pordes, R., Prosapio, A., Rechenmacher, R., Quinn, T. R., Richards, G. T., Richmond, M. W., Rivetta, C. H., Rockosi, C. M., Ruthmansdorfer, K., Sandford, D., Schlegel, D. J., Schneider, D. P., Sekiguchi, M., Sergey, G., Shimasaku, K., Siegmund, W. A., Smee, S., Smith, J. A., Snedden, S., Stone, R., Stoughton, C., Strauss, M. A., Stubbs, C., SubbaRao, M., Szalay, A. S., Szapudi, I., Szokoly, G. P., Thakar, A. R., Tremonti, C., Tucker, D. L., Uomoto, A., Berk, D. V., Vogeley, M. S., Waddell, P., Wang, S., Watanabe, M., Weinberg, D. H., Yanny, B., , and Yasuda, N. (2000), "The Sloan Digital Sky Survey: Technical Summary," *The Astronomical Journal*, 120, 1579–1587.